RSC Advances

ROYAL SOCIETY OF CHEMISTRY

www.rsc.org/advances

Journal Name

RSCPublishing

ARTICLE

Facile Synthesis of Meso-structured Pd/FeO_x and Its Highly Catalytic Performance for Low Temperature CO Oxidation under Ambient Condition

Cite this: DOI: 10.1039/x0xx00000x

Received 00th January 2012,
Accepted 00th January 2012

DOI: 10.1039/x0xx00000x

www.rsc.org/

Liang Li*, Gengnan Li‡, Yuan Yuan‡, Yongsheng Li

A series of meso-structured Pd/FeO_x catalysts were successfully fabricated through a facile pyrolysis and in-situ reduction strategy. The as-prepared materials possessed relative high surface area and highly dispersed Pd species, and exhibited excellent low temperature CO oxidation properties under ambient condition. Complete CO conversion could be achieved at as low as -5 ^oC, when 2.5 vol% H_2O was introduced into the feed gas. *In-situ* DRIFT analysis proved that this excellent catalytic properties can be attributed to the promotion of the water molecules and the synergetic effect between Pd nanoparticles and meso-structured FeOx support.

Introduction

Low temperature CO oxidation has been studied extensively in the past two decades due to its great importance for both practical application and fundamental research.[1-6] In practical applications, especially for automotive emission controlling process, large amount of CO are usually generated during the cold start period, entering the air within exhaust emissions and thus causing serious environmental problem. Therefore, it is of great necessity to regulate CO emission or even eliminate the diluted CO in the polluted air by developing efficient catalysts that convert CO into CO_2 under ambient condition. Although many catalytic systems for low temperature CO oxidation have been well developed in recent years, most of them are easily deactivated by the moisture.[7-18] Recent studies have suggested that platinum metals have much higher water residence during CO oxidation process. Thus, much attention has been focused on the supported noble metal catalyst, especially the supported Pd(O) catalyst.[19-23]

It is well known that the synergism between active component and support plays an important role in determining the catalytic performance. Benefited from the various oxidation states, charge-variable transition metal oxide possesses excellent performance in oxygen storage and release which is also critical factor for low temperature CO oxidation. When combined with Pd nanoparticles, significantly enhanced activity could be achieved especially under moisture conditions. This has been well proved in our previous studies.[24,25] In the mixed iron oxide, there is two different oxidation state ferrum ions, which not only benefit its electron transferring, but also possess much higher oxygen storage and release capacity. Recently, Deng et al. reported that $Fe(OH)_x$ or FeO_x supported Pd catalyst were more active for low temperature CO oxidation reaction under dry condition.[26] It is therefore expected that mesoporous FeO_x supported Pd catalyst should give the excellent catalyst for CO oxidation under moisture condition.

In this work, meso-structured FeO_x support was synthetized through the facile thermal decomposition of oxalate precursor FeC_2O_4•$2H_2O$. The palladium nanoparticles were successfully and homogeneously loaded by an improved wet impregnation with an in-suit reduction protocol. The as-prepared materials possessed relatively high specific surface area and the palladium nanoparticles were homogeneously dispersed in the mesoporous support. The catalytic activity of prepared Pd/FeO_x materials with different Pd loading contents were measured under dry and moisture condition, respectively.

Experimental

Material preparation

10 mmol $FeSO_4 \cdot 7H_2O$ was first dissolved in 100 ml aqueous solution, then 10 ml 1 M oxalate was slowly added under vigorous stirring. The resulting precipitate was filtered, washed with deionized water and dried at 60 ^oC for 24 h. The mesporous FeO_x support was obtained after calcinated at 250 ^oC for 2h.

A series of FeO_x supported Pd catalysts with different loading content were synthesized through an improved wet impregnation method. In a typical synthesis, 1 g mesoporous FeO_x material was added in 20 ml aqueous solution containing desired content of Na_2PdCl_4. After stirred for 2 h, 500 ml 0.1 M hydrazine hydrate ($NH_2NH_2 \cdot H_2O$) was added dropwise under vigorous stirring. The resulting precipitate was centrifuged,

washed several times with deionized water and dried at 60 °C for 24h.

Characterization

Powder X-ray diffraction was measured on a Bruker D8 Focus powder diffract meter with graphite monochromatized Cu Kα radiation (λ=0.15405 nm) operated at 40 kV. Thermo gravimetric analysis (TG–DSC) was recorded from ambient temperature to 800 °C at a heating rate of 10 °C /min with an air flow rate of 20 ml/min^{-1}. Nitrogen adsorption and desorption isotherms were obtained by a Micromeritics TriStar II 3020 analyzer at 77K. The specific surface area and pore size distribution were calculated using the Brunauer-Emmett-Teller (BET) and Barrett-Joyner-Halenda (BJH) methods, respectively. High-Resolution Transmission Electron Microscopy (HRTEM) observations were performed on a field emission JEM-2100 (JEOL) electron microscope operated at 300 kV equipped with a Gatan-666 electron energy loss spectrometer and energy dispersive X-ray spectrometer. XPS (X-ray photoelectron spectroscopy) signals were collected on a VG Micro MK II instrument using monochromatic Al Kα X-ray at 1486.6 eV operated at 200 W. All the elemental binding energies were referenced to the C (1s) line situated at 284.6 eV. H_2 temperature programmed reduction (H_2-TPR) analysis was performed by using a Micromeritics ChemiSorb 2750 apparatus. *In-situ* diffuse reflectance infrared fourier transform spectroscopy (DRIFTS) spectra were recorded by a FTIR spectrometer (Nicolet iS10) equipped with a MCT detector. The sample cell was fitted with ZnSe windows. The sample was exposed to the corresponding reactive stream (60 ml min^{-1}). The DRIFTS spectra obtained at 25 °C with a solution of 4 cm^{-1} and 50 scans. Typical gas mixture was 0.5 vol% CO, 20.0 vol% O_2 balanced with He. Water vapor was carried into the gas mixture by a bubbler in a water bath at room temperature. After a designated amount of time, the CO flow was switched to a humid stream containing 1.5 vol% water.

Catalytic activity test

The catalytic activity for CO oxidation was measured in fixed-bed quartz tubular reactor (i.d = 6 mm) containing 100 mg of catalyst without any pretreatment. A mixture contained 1.0 vol% CO, 20.0 vol% O_2 and high-purity N_2 (99.99%) was used as source gas. The feed gas at a flow rate of 25ml.min^{-1} was introduced into the reactor using mass-flow controllers, corresponding to a space velocity of 15000 ml·h^{-1}·g^{-1}. The conversion of CO was calculated by online gas chromatograph (GC). The reaction temperature was monitored through a thermocouple installed in the catalyst bed. The catalytic activity in moisture condition was tested by passing the feed gas at a flow rate of 75 ml·min^{-1} through a water vapor saturator.

Results and discussion

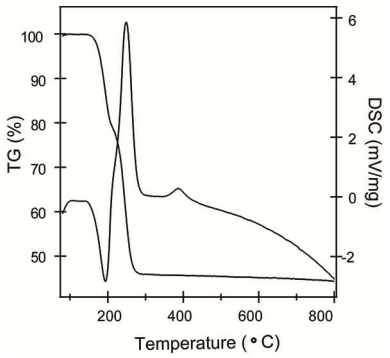

Fig.1 The TG-DSC curves of the $FeC_2O_4 \cdot 2H_2O$ precursor

Meso-structured FeO_x support was fabricated directly through controlled thermal decomposition of ferrous oxalate. The decomposition process has a strong effect on crystallite size and the texture of the product, in addition to the catalytic activities. In order to determine an appropriate temperature for calcination, the thermal behaviour of the ferrous oxalate precursor was first investigated by TG-DSC analysis in a static air atmosphere at a heating rate of 10 °C/min, as shown in Fig. 1. From ambient temperature to 800 °C, the oxalate precursor lost 54% of its original weight in three steps accompanied by two endothermic and two exothermic process. The first two endothermic peak occurring at about 78 °C and 195 °C correspond to the elimination of absorbed and coordinated water in the precursor, respectively. Further increasing the temperature to 230 °C, there is a rapid weight loss companied with a strong exothermic peak in the DSC line, suggesting the decomposition of the oxalate into crystalline FeO_x and the combustion of the decomposition product. The little exothermic peak at 400 °C in the DSC line should be contributed to the phase transformation between different Fe oxides. The temperature for calcination was determined at 250 °C in the experiment to get the meso-structured mixed phase FeO_x support.

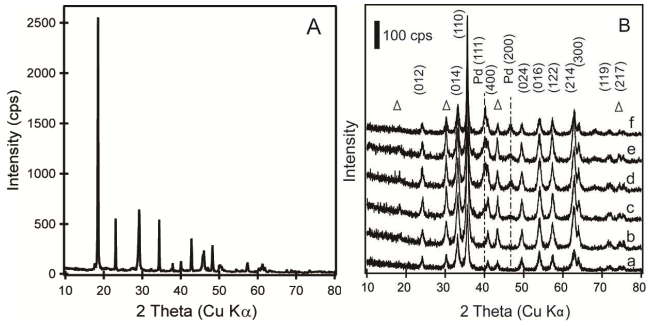

Fig. 2 The XRD patterns of $FeC_2O_4 \cdot 2H_2O$ precursor (A) and Pd/FeO_x catalysts with different Pd loading contents (B): 0 wt% (a), 1.1 wt% (b), 3.3 wt% (c), 5.8 wt% (d), 7.1 wt% (e) and 9.0 wt% (f)

Crystal phase composition

Fig. 2A depicts the powder X-ray diffraction (XRD) pattern of the ferrous oxalate precursor, a series of sharp and symmetrical

Bragg diffraction peaks can be found in the wide angle area, which demonstrates the well crystallized feature. After calcined at 250 °C for 2h, the ferric oxalate precursor was completely decomposed and converted to ferric oxide. (Fig. 2B). It clearly shows that the main components of the resulting oxide are hematite (Fe_2O_3). Besides, some weak peaks marked with triangle appearing at 2θ = 30.2°, 35.5°, 43.2°, 47.2° also indicate the existence of Fe_3O_4. When loaded with Pd, two peaks emerged at 2θ = 40 ° and 46 °, which could be identified as (111) and (200) diffraction bands of face-centered cubic structure palladium, respectively. Diffraction intensity increased with the increase of Pd loading content. It should be noted that all the characteristic peaks of metallic Pd were broad and weak, indicating highly dispersed amorphous or small palladium nanoparticles. However, due to the partial overlapping between diffraction peaks of Pd (111) and Fe_2O_3 (004), it is difficult to estimate palladium particle size from Pd (111) using the Scherrer equation. The actual contents of Pd loaded in the meso-structured Pd/FeO_x materials were determined by the ICP-AES technique to be 1.1wt%, 3.3wt%, 5.8wt%, 7.1wt%, 9.0wt%.

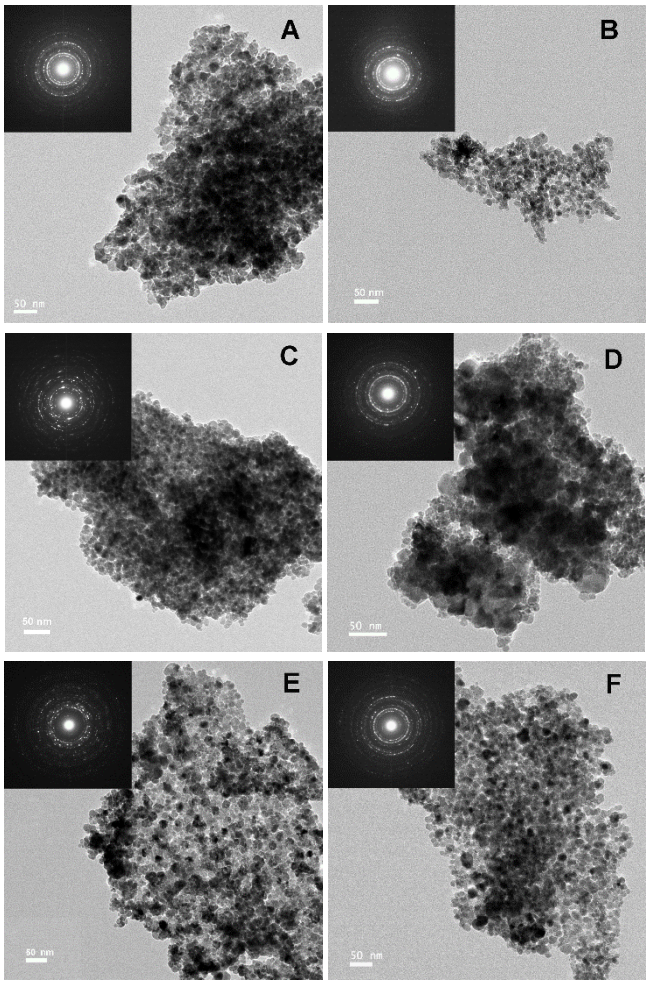

Fig. 3 The TEM images of the Pd/FeO_x catalysts with different Pd loading contents: 0 wt% (A), 1.1wt% (B), 3.3 wt% (C), 5.8 wt% (D), 7.1wt% (E) and 9.0 wt% (F)

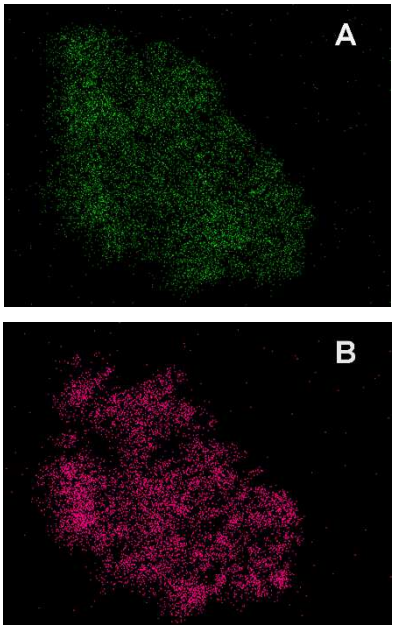

Fig. 4 The Element Mapping images of Pd/FeO_x catalyst: Fe (A), Pd (B)

Morphology, pore structure and surface area

To get more explicit details, transmission electron microscopy (TEM) were carried out to observe the morphology of Pd/FeO_x and the distribution of Pd in the materials (Fig. 3). For FeO_x support, 10-15 nm nanoparticles uniformly aggregated together to form the meso-pore, which were generated from the decomposition and mass loss of ferrous oxalate hydrate crystals during pyrolysis. The sequential impregnation and reduction process did not affect its porous structure. When loaded with palladium, there is not any large particles in the TEM images and the noble metal nanoparticles cannot be well distinguished, suggesting that the Pd species have been highly dispersed into or on the mesoporous FeO_x support. The insets are selected area electron diffraction (SAED) patterns from the same area. The well-defined diffraction rings for Fe_2O_3 and Fe_3O_4 can be found in all the samples. Instead, the relative faint and disintegrated diffraction ring for Pd indicates its very low crystallinity and /or small size and only can be found when Pd loading content higher than 3.3 wt%, which is consistent well with above XRD result. The further high resolution transmission election microscopy (HRTEM) investigation clearly shows that the catalysts are composed of crystallized FeO_x and poorly crystallized palladium nanoparticles (ESI†). The Element Mapping images in Fig. 4 provide a further overall observation of element distribution. The two different colours represent two kinds of element (Fe, Pd) respectively. The palladium nanoparticles has been highly dispersed into/on mesoporous supports.

The texture properties of the materials were investigated by measuring adsorption and desorption isotherms of nitrogen at 77K, as shown in Fig. 5. In all the cases, the typical Langmuir IV isotherms suggest the mesoporous structure and the appearance of H3 hysteresis loops indicates the formation of slit-like mesopores, which were generated from the

decomposition and mass loss of oxalate hydrate precursor during the pyrolysis. The specific surface area of the materials was calculated by Brunauer-Emmet-Teller (BET) equation and the inset shows the pore size distribution obtained through the Barrett-Joyner-Halenda (BJH) method. The specific surface areas are all located within 60-70 m^2/g and the main pore sizes are all centred at about 10 nm, confirms that the loading of Pd did not change the mesoporous structure nature of FeO_x support. Furthermore, it is worth noting that there is only a little limited change in the specific surface area and pore size with the increase of Pd loading amount, indicates the uniformly dispersion of palladium nanoparticles.

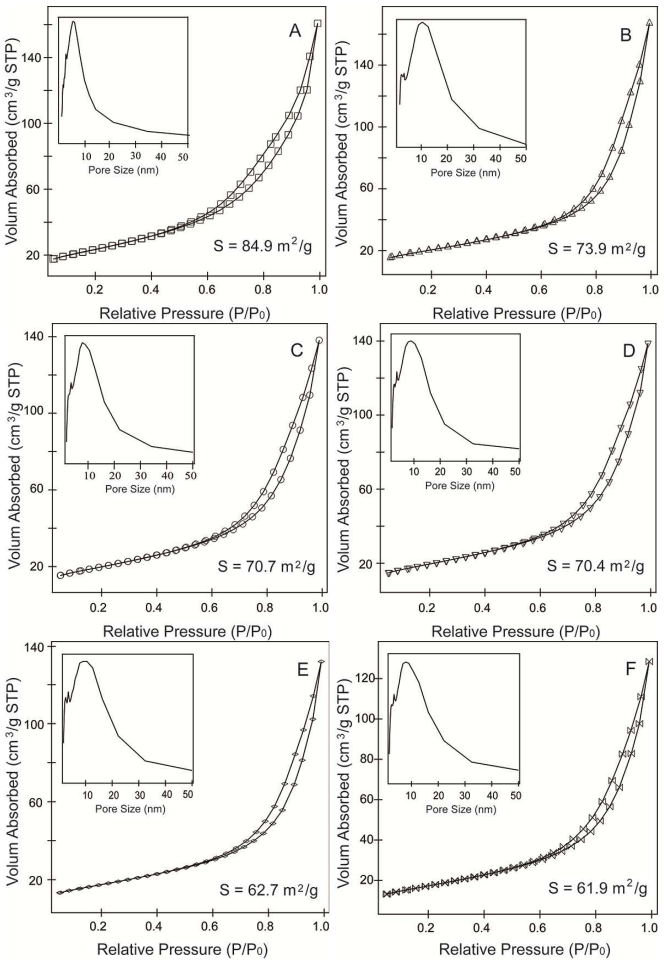

Fig. 5 The N_2 adsorption-desorption analysis of the FeO_x support (A) and the Pd/FeO_x catalysts with different Pd loading contents: 1.1 wt% (B), 3.3 wt% (C), 5.8 wt% (D), 7.1 wt% (E) and 9.0 wt% (F)

Surface composition, metal oxidation state

The XPS measurements were performed to detect the surface chemical states of the FeO_x support and 7.1 wt% Pd loaded Pd/FeO_x catalyst with and without catalytic performance. In all the cases, carbon C1s core excitation at binding energy of 284.6 eV was taken as reference. The Fe 2p XPS spectra are shown in the Fig. 6A. There are two prominent peaks at binding energy of 711.0 eV and 724.6 eV which are recognized as Fe $2p_{2/3}$, Fe $2p_{1/2}$ respectively.[27-30] Meanwhile, they both have satellite peaks: 718.5 eV for Fe $2p_{2/3}$ and 732.8 eV for Fe $2p_{1/2}$. The Fe $2p_{2/3}$ spectrum can be deconvoluted into three components at binding energy of 709.7 eV, 710.8 eV and 713.5 eV, represent Fe^{2+} octahedral, Fe^{3+} octahedral and Fe^{3+} tetrahedral, respectively.[31-33] It clearly indicates the co-existence of Fe^{2+} and Fe^{3+} on the surface of the material. Fig. 6B shows the O1s XPS spectra which can be resolved into two peaks: lattice oxygen (O_{latt}) at 529.6 eV and surface adsorbed oxygen (O_{ads}) at 531.4 eV.[34] The amount of lattice oxygen decreased as the palladium loaded which can be attributed to the more absorbed oxygen on the high dispersed palladium species. Moreover, Pd 3d XPS spectra are obtained in Fig. 6C. The typical binding energy of Pd^0 and Pd^{2+} states are 335.1 eV, 336.7 eV, 340.4 eV and 342.1 eV, respectively.[35-37] It is worth to point out that most of palladium exists as Pd^0 in the Pd/FeO_x catalyst. However, after catalyst test, the component of Pd^{2+} increased probably due to the oxidation of Pd^0 in the process of catalytic performance.

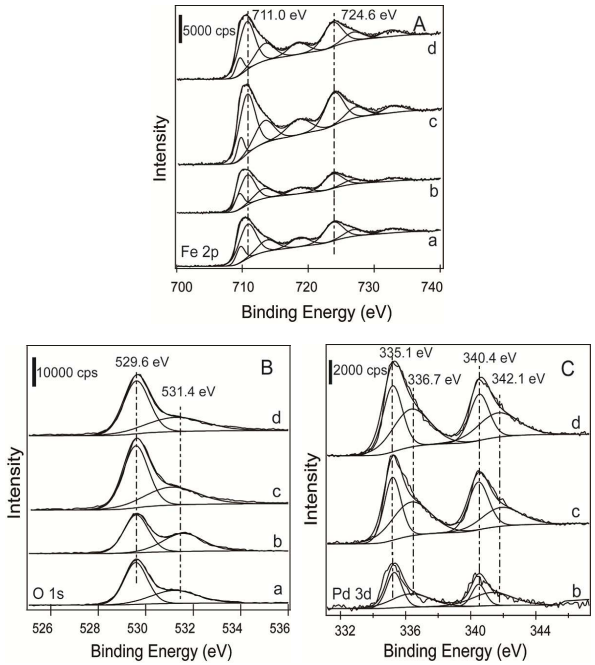

Fig. 6 The XPS spectra of the FeO_x support (a) and 7.1 wt% Pd/FeO_x catalyst before reaction (b), after reaction under dry condition (c) and after reaction under moisture condition (d)

Catalytic properties

Fig. 7 shows the reduction profiles of the catalysts. For comparison, the H_2 temperature programmed reduction (H_2-TPR) profile of the parent FeO_x is also included. The TPR profile of FeO_x is consisted of two distinguishable reduction regions. One peak at about 320 ^oC can be assigned to the reduction of Fe_2O_3 to Fe_3O_4. The other broad signal at 450-750 ^oC is the reduction of Fe_3O_4 to Fe^0. After loaded with palladium, the reduction peak is obviously shifts to the relative lower temperature region. The significant low-temperature reduction feature strongly suggests that the FeO_x substrate has

been 'activated' to a large extent in the Pd/FeO_x catalyst by Pd loading.

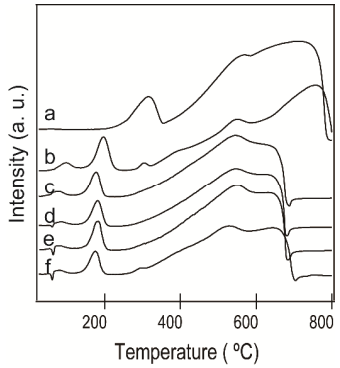

Fig. 7 The H_2-TPR profiles of FeO_x (a) and Pd/FeO_x catalysts with different Pd loading contents 1.1 wt% (B), 3.3 wt% (C), 5.8 wt% (D), 7.1 wt% (E) and 9.0 wt% (F)

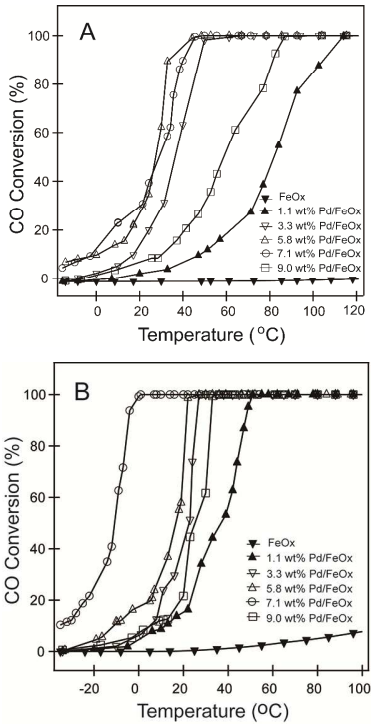

Fig. 8 The catalytic performance of FeO_x and Pd/FeO_x under different reaction conditions: (A) dry condition, (B) moisture condition (The water concentration in the feed gas is 2.5 vol% H_2O)

The catalytic performances of Pd/FeO_x catalysts for CO oxidation under different reaction conditions are shown in Fig. 8. The FeO_x support does not show any catalytic activity with the reaction temperature lower than 100 °C under dry condition. When loaded with palladium, the catalytic activity shows a significant improvement. As Pd content reached to 7.1 wt%, the CO full conversion temperature decreased as low as 47 °C. Continuous increase the Pd content does not show better catalytic activity. The catalytic activity of Pd/FeO_x catalyst is not only determined by the active component, but also the geometric structures of FeO_x support and the synergy between palladium and FeO_x.[29-31] Generally, moisture is inevitable existence during practical application for CO elimination. It is more important to explore the catalytic performance under ambient condition. Surprisingly, the catalytic activity of Pd/FeO_x does not get worse but a significantly enhancement under the moisture condition (Fig. 8B). 7.1 wt% Pd/FeO_x catalyst still show the highest catalytic activity. The CO full conversion temperature can be decreased as low as 0 °C, when 2.5 vol% H_2O was introduced into the feed gas. It clearly suggests the appropriate moisture is beneficial to the CO oxidation when Pd/FeO_x was used as catalyst. Moreover, to gain insight into the intrinsic activities of supported Pd catalysts, TOFs normalized by the number of the surface noble atoms under differential reaction conditions were calculated. No matter under the dry or moisture condition at 0 °C, The TOFs of the 7.1 wt% Pd loaded catalyst all give the maximum values (1.41×10^{-4} s^{-1} under dry condition and 27.9×10^{-4} s^{-1} under moisture condition, respectively) among all samples synthesized.

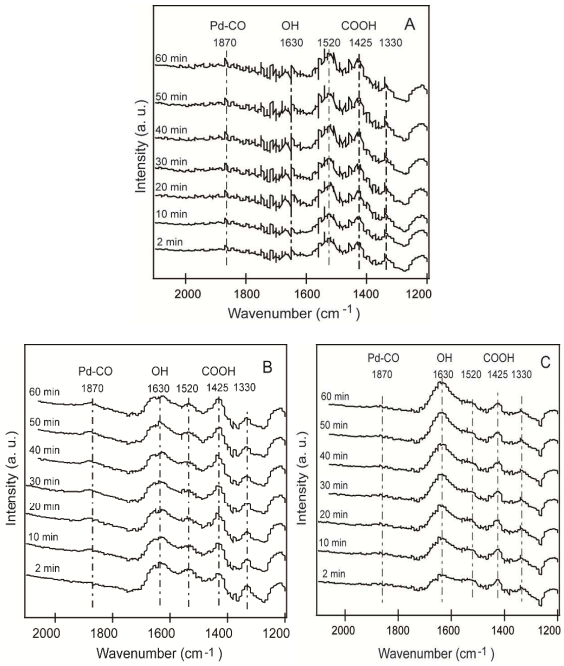

Fig. 9 *In-situ* DRIFTS spectra of 7.1 wt% Pd/FeO_x under(A) 0.5 vol% CO -He (B) 0.5 vol% CO-20 vol% O_2-He and (C) 0.5 vol% CO-20 vol% O_2-1.5 vol% H_2O-He at 25 °C.

In-situ DRIFTS measurements

To further determine the effect of water during CO oxidation process, *in-situ* DRIFTS technology was employed to explore the difference of surface reaction of CO on 7.1 wt% Pd/FeO_x catalyst under different reaction conditions. According to the literatures, the wide bands at 1360 and 1470 cm^{-1} are ascribed to υ_s(OCO) and δ(OH) of $[COOH]_s$, respectively.[32-34] The strong band at 1600-1700 cm^{-1} can be assigned to the OH groups,[35,36] whereas, the weak band at 1810 cm^{-1} is related to bonded CO on metallic Pd.[37,38] Interestingly, once Pd/FeO_x was exposed to 0.5 vol% CO, [COOH] species was formed immediately and the peak intensity gradually increase in the

absence of water and O_2, which indicates that CO directly reacts with the surface hydroxyl on Pd/FeO_x catalyst to form [COOH] intermediates (Fig. 9A). When 20.0 vol% O_2 was introduced into the feed gas (dry condition, Fig. 9B), the bands at 1650 cm^{-1} attributed to surface -OH gradually decreased with the contact time, which further prove the surface –OH group participation in the CO oxidation process. In contrast, under the moisture condition (Fig. 9C), due to the adequate supply of -OH, the intensity of –OH group remains relatively constant during the whole process. Besides, compared with that under dry stream, Pd-CO band appear and become stable more rapidly. The presence of water could not only be in favor of a formation of carbonate species (COOH), but also promote the adsorption of CO on the surface of metallic Pd. All these clearly indicate the positive effect of water in CO oxidation on the surface of Pd/FeO_x catalysts.

Conclusions

In summary, the crystalline mesoporous Pd/FeO_x catalysts were successfully fabricated through an improved impregnation protocol. The as-prepared materials owned good crystallinity, relatively high specific surface area and highly dispersed Pd nanoparticles, and exhibited excellent low temperature CO oxidation properties under ambient condition. Complete CO conversion could be achieved at as low as -5 ^oC for 7.1 wt% Pd loaded catalyst, when 2.5 vol% H_2O was introduced into the feed gas. In-situ DRIFTS analysis proved the positive effect of water during CO oxidation process.

Acknowledgements

This study was supported by National Basic Research Program of China 2013CB933201.

Notes and references

*Key Laboratory for Ultrafine Materials of Ministry of Education, School of Materials Science and Engineering, East China University of Science and Technology, Shanghai 200237, China

E-mail: liliang@ecust.edu.cn Tel: +86-21-64252599; Fax: +86-21-64250740

‡ Yuan Yuan and Gengnan Li contribute equally to this work.

†Electronic Supplementary Information (ESI) available: [HRTEM images of the Pd/FeOx materials with different Pd content and the detailed XPS analysis result for 7.1 wt% Pd loaded Pd/FeOx catalyst]. See DOI: 10.1039/b000000x/

1 M. Haruta, N. Yamada, T. Kobayashi, S. Iijima, *J. Catal.* 1989, **115**, 301.

2 M. S. Chen, D.W. Goodman, *Science* 2004, **306**, 252.

3 C. T. Campbell, *Science* 2004, **306**, 234.

4 A. U. Nilekar, S. Alayoglu, B. Eichhorn, M. Mavrikakis, *J. Am. Chem. Soc.* 2010, **132**, 7418.

5 A. Hadi, I. Yaacob, *Catal. Today* 2004, **96**, 165.

6 J. Huang, S.Wang, Y. Zhao, X. Wang, S. Wang, S. Wu, S. Zhang, W. Huang, *Catal. Commun.* 2006, **7**, 1029.

7 M. Date, M. Okumura, S. Tsubota, M. Haruta, *Angew. Chem. Int. Ed.* 2004, **43**, 2129.

8 R. A. Ojifinni, N.S. Froemming, J. Gong, M. Pan, T.S. Kim, J.M. White, G. Henkelman, C.B. Mullins, *J. Am. Chem. Soc.* 2008, **130**, 6801.

9 H. H Kung, M.C. Kung, C. K. Costello, *J. Catal.* 2003, **216**, 425.

10 M. Date, H. Imai, S. Tsubota, M. Haruta, *Catal. Today* 2007, **2**, 225.

11 H. Yen, Y. Seo, S. Kaliaguine, F. Kleitz, *Angew. Chem. Int. Ed.* 2012, **51**, 12032.

12 J. Zhu, Q. Gao, *Micro. Meso. Mater.* 2009, **124**, 144.

13 X. Xie, L. Li, Z.-Q. Liu, M. Haruta, W. Shen, Nature 2009, **458**, 746.

14 Y. Feng, L. Li, S. Niu, Y. Qu, Q. Zhang, Y. Li, W. Zhao, H. Li, J. Shi, *Appl. Catal. B Environ*. 2012, **111**, 461.

15 L.-N. Cai, Y Guo, A.-H. Lu, P. Branton, W.-C. Li, *J. Mol. Catal. A: Chem.* 2012, **360,** 35.

16 S. A. Kondrat, T. E. Davies, Z. Zu, P. Boldrin, J.K. Bartley, A.F. Carley, S.H. Taylor, M.J. Rosseinsky, G.J. Hutchings, *J. Catal.* 2011, **281**, 279.

17 R. Xu, X. Wang, D. Wang, K. Zhou, Y. Li, J Catal. 2006, **237**, 426.

18 E. C. Njagi, C. H. Chen, H. Genuino, H. Galindo, H. Huang, S.L. Suib, *Appl. Catal. B Environ.* 2010, **99**,103.

19 B. Qiao, L. Liu, J. Zhang, Y. Denga, *J. Catal.* 2009, **261**, 241.

20 L. Liu, F. Zhou, L. Wang, X. Qi, F. Shi, Y. Deng, *J. Catal.* 2010, **274**, 1.

21 L.-C. Wang, Q. Liu, X.-S. Huang, Y.-M. Liu, Y. Cao, K.-N. Fan. *Appl. Catal. B Environ.* 2009, **88**, 204.

22 A. V. Salker, R.K. Kunkalekar, *Catal. Commun.* 2009, **10**, 1776.

23 J. S. Park, D.S. Doh, K.Y. Lee, *Top. Catal*. 2000, **10**, 127.

24 G. Li, L. Li, Y. Yuan, J. Shi , Y. Yuan, Y. Li, W. Zhao, J. Shi, *Appl. Catal. B Environ.* 2014, **158-159**, 34.

25 G. Li, L. Li, Y. Yuan, J. Shi , Y. Yuan, Y. Li, W. Zhao, J. Shi, *RSC Adv.* 2014, **4**, 35762.

26 L. Liu, B. Qiao, Y. He, F. Zhou, B. Yang, Y. Deng, *J. Catal.* 2012, **294**, 29.

27 X. W. Xie, L. Li, Z.-Q. Liu, M. Haruta, W.J. Shen, *Nature* 2009, **458**, 746.

28 M. Dat, M. Okumura, S. Tsubota, M. Haruta, *Angew. Chem. Int. Ed.* 2004, **43**, 2129.

29 R.V. Gulyaev, A.I. Stadnichenko, E.M. Slavinskaya, A.S. Ivanova, S.V. Koscheev,A.I. Boronin, *Appl. Catal. A: Gen.* 2010, **439–440**, 41.

30 A. Trovarelli, *Catal. Rev.-Sci. Eng.* 1996, **38**, 439.

31 J.L. Shi, *Chem. Rev.* 2013, **113**, 2139.

32 B. B. Chen, C. Shi, M. Crocker, Y. Wang, A. M. Zhu, *Appl. Catal. B: Environ.* 2013, **132-133**, 245.

33 Y. Denkwitz, A. Karpenko, V. Plazk, R. Leppelt, B. Schumacher, R. J. Behm, *J. Catal.* 2007, **246**, 74.

34 S. Zhang, X. Li, B. Chen, X. Zhu, C. Shi, A. M. Zhu, *ACS Catal.* 2014, **4**, 3481.

35 K. I. Choi and M. A. Vannice, *J. Catal.* 1991, **127**, 465.

36 K. I. Choi and M. A. Vannice, *J. Catal.* 1991, **131**, 36.

37 S. D. Ebbesen, B. L. Mojet, L. Lefferts, *Phys. Chem. Chem. Phys.* 2009, **11**, 641.

38 G. Rupprechter, H. Unterhalt, M. Morkel, P. Galletto, L. J. Hu, H. *J. Freund, Surf. Sci.* 2002, **502**, 109.

